

Skin-Friction and Forced Convection from an Isothermal Rough Plate

Aubrey G. Jaffer
e-mail: agj@alum.mit.edu

Abstract

A novel analysis of the turbulence generated by flow over self-similar roughness yields new correlations for skin-friction coefficient and forced convection from an isothermal plate having root-mean-squared height-of-roughness ε :

$$f_c = \frac{1}{3 \ln^2(L/\varepsilon)} \quad \text{Nu} = \frac{\text{Re Pr}^{1/3}}{6 \ln^2(L/\varepsilon)}$$

Convection measurements of a self-dissimilar bi-level plate having precisely 3 mm of roughness match this convection correlation within 3% at Reynolds numbers from 5000 to 50000.

An analysis of the original sand-roughness experiments finds that its relation to root-mean-squared height-of-roughness is nonlinear. The resulting scale error explains discrepancies between the Prandtl and Schlichting formula, two more recent papers, and the formulas developed here.

Convection measurements of a bi-level plate imply a tighter upper bound for the height of admissible-roughness:

$$k_{adm} = 29 \frac{L}{\text{Re}}$$

Keywords: skin-friction; profile roughness; sand-roughness; admissible-roughness; forced-convection; turbulence

Table of Contents

<i>Introduction</i>	2
<i>Prior Work</i>	3
<i>Roughness</i>	4
<i>Self-Similar Profile Roughness</i>	5
<i>Self-Similar Surface Roughness</i>	6
<i>Vertical Roughness Travel</i>	7
<i>Skin Friction</i>	8
<i>Self-Dissimilar Roughness</i>	10
<i>Transitional Rough Regime</i>	11
<i>Sand Roughness</i>	12
<i>Admissible Roughness</i>	14
<i>Roughness in Pipes</i>	15
<i>Conclusion</i>	15
<i>Nomenclature</i>	16
<i>Greek Symbols</i>	16
<i>References</i>	17
<i>Appendix: Rough to Smooth Turbulence Transition</i>	18

1. Introduction

Predicting the skin-friction of a rough surface is important to the fluid dynamics of vehicles and turbines. The related phenomenon of convection from a rough surface has application to modeling weather and the thermal behavior of buildings.

Skin-friction of a plate with a rough surface is different in character from skin-friction of a smooth flat surface because the roughness protrudes through what would otherwise be a laminar boundary layer adjacent to the plate. This creates a type of turbulent flow which Prandtl and Schlichting[1] term “the completely rough regime”, and Schlichting’s *Boundary-layer theory*[2] calls “fully turbulent”.

Prandtl and Schlichting assert that the plate’s height-of-roughness decreases relative to the depth of the boundary layer growing along the plate in the direction of flow. This would not be true of a surface with self-similar roughness (defined in Section 3). The ratio of height-of-roughness to characteristic-length of the plate would be constant; thus the entire plate would be adjacent to fully turbulent flow.¹

Prandtl and Schlichting break their analysis into four regions based on this ratio. This is unnecessary with the self-similar roughness employed by the present work. This self-similar assumption is so clarifying that this new analysis of turbulence from surface roughness is independent of boundary-layer theory.

Another contention with prior work is that turbulent skin-friction can occur adjacent to plates under isobaric conditions, but flow in pipes is not isobaric.² Previous works have applied the methods of pipe flow analysis to rough plates. The present work is developed without appeal to pipe flow, although conversions between roughness metrics appear to work the same for pipes and plates.

Section 2 describes prior works and elucidates a problem with the commonly used sand-roughness metric.

Section 3 defines profile and surface roughness, the root-mean-squared (RMS) height-of-roughness metric, and a type of self-similarity for profile roughness functions. For self-similar profile roughness functions, the ratio of characteristic-length L to RMS height-of-roughness is constant over the profile.

This is of interest because Prandtl and Schlichting[1] teach that for rough plates at large Reynolds numbers (Re) “in the completely rough regime”, the friction coefficient f_c is a function only of the ratio of the characteristic-length of the system to the height-of-roughness. If this ratio is constant over the plate, then f_c will be constant over the plate.

Section 4 gives three examples of discrete self-similar profile roughness functions; and Section 5 shows the surfaces generated by perpendicularly combining each discrete profile function with itself.

Section 6 derives a formula for the total vertical travel of a conforming flow for two of the discrete profile roughness functions from Section 4. The ratio of vertical roughness travel to horizontal travel is used to scale the bulk fluid velocity to the roughness velocity.

Section 7 formulates skin-friction as the square of the ratio of roughness velocity to bulk fluid velocity.

In *Self-Similar Processes Follow a Power Law in Discrete Logarithmic Space*[3] Newberry and Savage demonstrate that some self-similar systems which are often modeled using continuous power-law probability distributions (such as the Pareto distribution) are better modeled using discrete power-law distributions.

The present work uses their idea in reverse. Conversion of flow into turbulence by contact with discrete self-similar roughness is derived; then the turbulence generation by continuous self-similar roughness is inferred using a random variable having a Pareto distribution.

Section 8 evaluates the resulting convection formula on a bi-level plate lacking self-similarity and finds that convection measurements of the plate match the new formula within 3% from $5000 < \text{Re} < 50000$.

Section 9 explores the low Re skin-friction behavior of rough plates, finding no dependence on Re. Section 12 explores its implications for roughness in pipes.

Section 10 examines the sand-roughness metric and its relations to RMS and arithmetic-mean roughness metrics, enabling comparisons with prior work.

Section 11 derives a threefold tighter upper bound for the height of admissible-roughness than is given in Schlichting’s book *Boundary-layer theory*[2].

The Section 17 appendix builds an intricate convection formula for the bi-level plate which models the transition from rough turbulent convection to smooth turbulent convection at increasing Reynolds numbers.

¹ Self-similar roughness is not possible in a pipe because its characteristic-length is the pipe diameter.

² Skin-friction causes the pressure to drop in the pipe.

2. Prior Work

In 1934 Prandtl and Schlichting published *Das Widerstandsgesetz rauher Platten (The Resistance Law for Rough Plates)*[1], which brilliantly infers a relation for skin-friction resistance for rough plates from their analysis of Nikuradse’s measurements of sand glued inside pipes. In *Boundary-layer theory*[2] Prandtl and Schlichting give a formula for fully rough (large Re) total skin-friction coefficient for a rough flat plate:

$$c_f = \left(1.89 + 1.62 \log_{10} \frac{L}{k_S}\right)^{-2.5} \quad 10^2 < L/k_S < 10^6 \quad (1)$$

In *On the Skin Friction Coefficient for a Fully Rough Flat Plate*[4], Mills and Hang present a formula they claim to be more accurate on the local skin-friction measurements done by Pimenta, Moffat, and Kays[5]. The corrected³ total skin-friction formula is:

$$C_D = \left(2.035 + 0.618 \ln \frac{L}{k_S}\right)^{-2.57} \quad (2)$$

Putting these formulas into similar form:

$$c_f = 2.41 \left(\ln \frac{14.68 L}{k_S}\right)^{-2.5} \quad C_D = 3.44 \left(\ln \frac{26.9 L}{k_S}\right)^{-2.57}$$

The roughness in both papers is reported in Nikuradse’s sand-roughness metric k_S , the height of “coarse and tightly placed roughness elements such as for example coarse sand grains glued on the surface”. Prandtl and Schlichting[1] gives the parameters of Nikuradse’s sand coatings:

Table 1 Nikuradse’s sand coatings

k_S	grains/cm ²	k_S^{-2}
.08 cm	150	156.25/cm ²
.04 cm	590	625/cm ²
.02 cm	1130	2500/cm ²
.01 cm	4600	10000/cm ²

Because their packing densities scale as the inverse square of grain size, the .08 cm and .04 cm sand coatings should scale correctly as long as the glue thickness is proportional to grain size. Similarly the .02 cm and .01 cm sand coatings should scale.

The two coarsest coatings (largest k_S values) had packing densities slightly less than a square packing. The other two had packing densities less than half that of a square packing. But comparing the .02 cm and .04 cm sand coatings, their packing density ratio is nearly 1:2, not 1:4. Thus formulas (1) and (2) will have incorporated a scale error (between measurements of large and small k_S) and should not be applied to L/k_S values much larger than 1000 (507 is the largest rough pipe R/k_S value in Schlichting[2] Fig. 20.18). Section 10 compares these formulas with the present work.

³ Mills and Hang’s published formula had a “6” where a “0” should have been in the first constant:

$$C_D = \left(2.635 + 0.618 \ln \frac{L}{k_S}\right)^{-2.57}$$

All of their measurement comparisons were of local skin-friction, which used a different formula. Their only use of the total skin-friction formula was a comparison with the Prandtl and Schlichting formula, which overstated the magnitude and negated the sign of that difference because of the error. Figure 13 shows traces for both the corrected and uncorrected formulas.

3. Roughness

Profile roughness is a function $z(x)$ where $0 \leq x \leq L$ is distance in the direction of flow.

Surface roughness is a function $z(x, y)$ of the x and y coordinates in the surface of the plate. There are no tunnels or overhangs. In order that the random fluid velocities resulting from interaction with the plate roughness are not skewed, $z(x, y)$ should be roughly isotropic; swapping x and y should not materially affect the behavior of the system. A surface composed of parallel ridges and valleys would not meet this criterion.

Consider the roughness profile $z(x)$ for a plate cut into strips parallel to the flow, each strip L long. The mean height \bar{z} and root-mean-squared height-of-roughness ϵ of the strip are:

$$\bar{z} = \frac{1}{L} \int_0^L z(x) dx \quad \epsilon = \sqrt{\frac{1}{L} \int_0^L [z(x) - \bar{z}]^2 dx} \quad (3)$$

The mean height and root-mean-squared height-of-roughness of surface roughness are:

$$\bar{z} = \frac{1}{L^2} \int_0^L \int_0^L z(x, y) dx dy \quad \epsilon = \sqrt{\frac{1}{L^2} \int_0^L \int_0^L [z(x, y) - \bar{z}]^2 dx dy} \quad (4)$$

These roughness functions need not be continuous to be integrable. Thus local flow properties may not be well-defined anywhere. Instead turn attention to the total flow over the strip.

A profile roughness function $z(x)$ has self-similar roughness with (integer) branching factor $n > 0$ if the RMS height-of-roughness of $z(x)$ over an interval $x_0 < x < x_n$ is n times the RMS height-of-roughness of $z(x)$ over each (evenly divided) sub-interval $x_j < x < x_{j+1}$ for $0 < j < n - 1$ at a succession of scales converging to 0.

Note that $z(x_j)$ values contribute to the interval height-of-roughness, but not to the sub-interval height-of-roughness.

If profile roughness function $z(x)$ has self-similar roughness, then the ratio of the length of the interval L to its RMS height-of-roughness ϵ will be invariant over that succession of scales converging to 0.

Self-similarity is of interest because the skin-friction coefficient f_c , which will be formulated in Section 7, is a function of L/ϵ . If the roughness is self-similar, then L/ϵ and $f_c(L/\epsilon)$ will be constant over the span of the roughness profile.

In the three examples of self-similar profile roughness in Section 4, the roughness is simply a permutation of the linear ramp $z(x) = x$ from $x = 0$ to $x = w$. Because the RMS height-of-roughness calculation depends only on the z values and not their relation to x , for all ramp-permutation profile roughness:

$$\epsilon = \sqrt{\frac{1}{w} \int_0^w [x - w/2]^2 dx} = \frac{w}{\sqrt{12}} \quad (5)$$

This leads to the question of whether a linear ramp, which fits this description of self-similarity, can cause turbulence. While vortexes can arise in two-dimensional flows, turbulence is a three-dimensional phenomena. The random velocity fluctuations must be isotropic at all but the coarsest length scales. Not only must the height profile be rough in the direction of flow, but perpendicular to the flow as well. This rules out simple ramps as rough profiles.

A linear ramp being disqualified, are self-similar roughness profiles possible?⁴ Section 4 constructs three examples of self-similar roughness profiles.

⁴ Flack, Schultz, Barros, and Kim[6] find that the shape of the roughness function (ΔU^+) for all fifteen of their grit-blasted surfaces shows self-similarity.

4. Self-Similar Profile Roughness

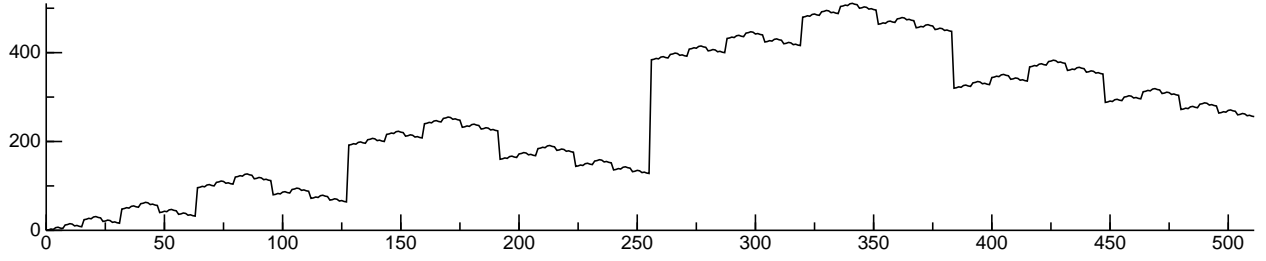


Figure 1 Gray-code profile roughness

The integer Gray-code sequence $G(x, w)$ with $0 \leq x < w = 2^j$ shown in Figure 1 has a RMS height-of-roughness $\epsilon = w/\sqrt{12}$ and is self-similar (when bisected) as seen by its recurrence:

$$G(x, w) = \begin{cases} x, & \text{if } w = 1; \\ w + G(w - 1 - (x \bmod w), w/2), & \text{if } \lfloor x/w \rfloor = 1; \\ G(x \bmod w, w/2), & \text{otherwise.} \end{cases} \quad (6)$$

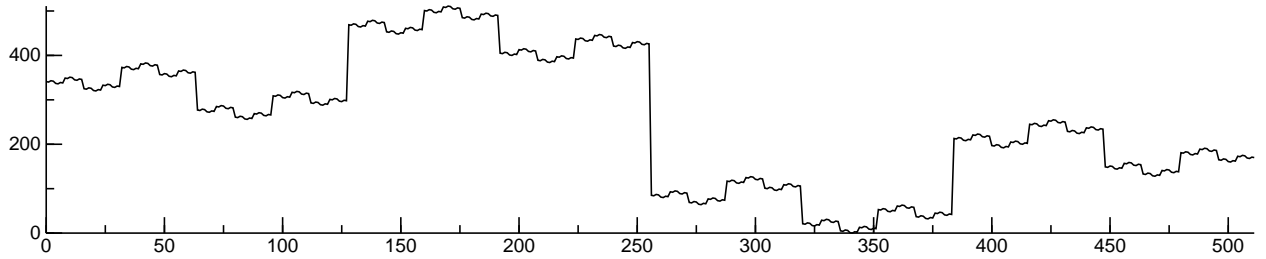


Figure 2 Wiggliest self-similar profile roughness

The integer sequence $W(x, w)$ which reverses at each bifurcation produces the wiggliest possible self-similar roughness with $0 \leq x < w = 2^j$ and is shown in Figure 2; it has a RMS height-of-roughness $\epsilon = w/\sqrt{12}$:

$$W(x, w) = \begin{cases} x, & \text{if } w = 1; \\ \lfloor x/w \rfloor w + W(w - 1 - (x \bmod w), w/2), & \text{otherwise.} \end{cases} \quad (7)$$

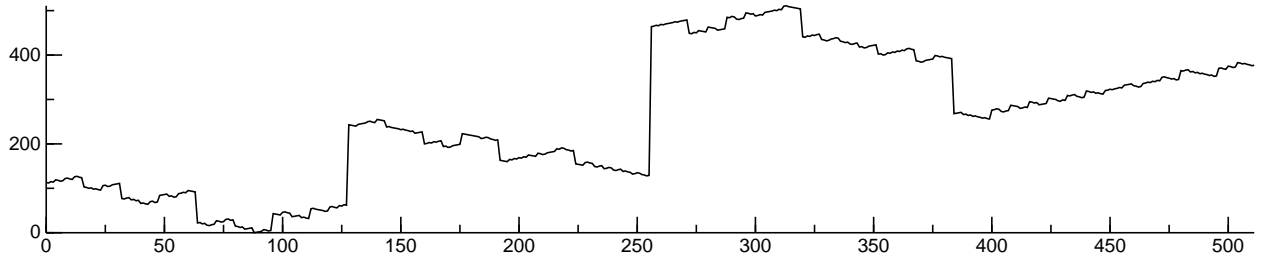


Figure 3 Randomly reversing bifurcation profile roughness

Figure 3 shows an integer sequence generated by recursive-descent with random reversing at each halving. It has a RMS height-of-roughness $\epsilon = w/\sqrt{12}$ and is approximately self-similar.

5. Self-Similar Surface Roughness

A $L \times L$ self-similar roughness function $z(x, y)$ can be constructed from a profile roughness function $Y(x, w)$:

$$z(x, y) = \frac{\varepsilon \sqrt{6}}{w} \left[Y\left(x \frac{w}{L}, w\right) + Y\left(y \frac{w}{L}, w\right) \right] \quad w = 2^j$$

For permutation profile roughness, the surface height-of-roughness ε is $\sqrt{2}$ times the profile height-of-roughness ϵ .

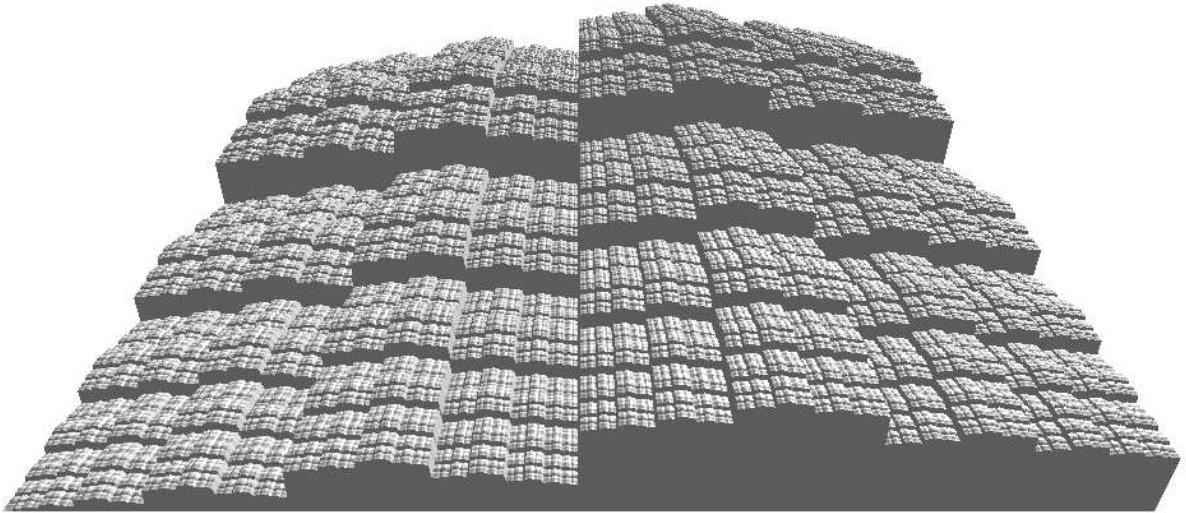


Figure 4 Gray-code surface roughness

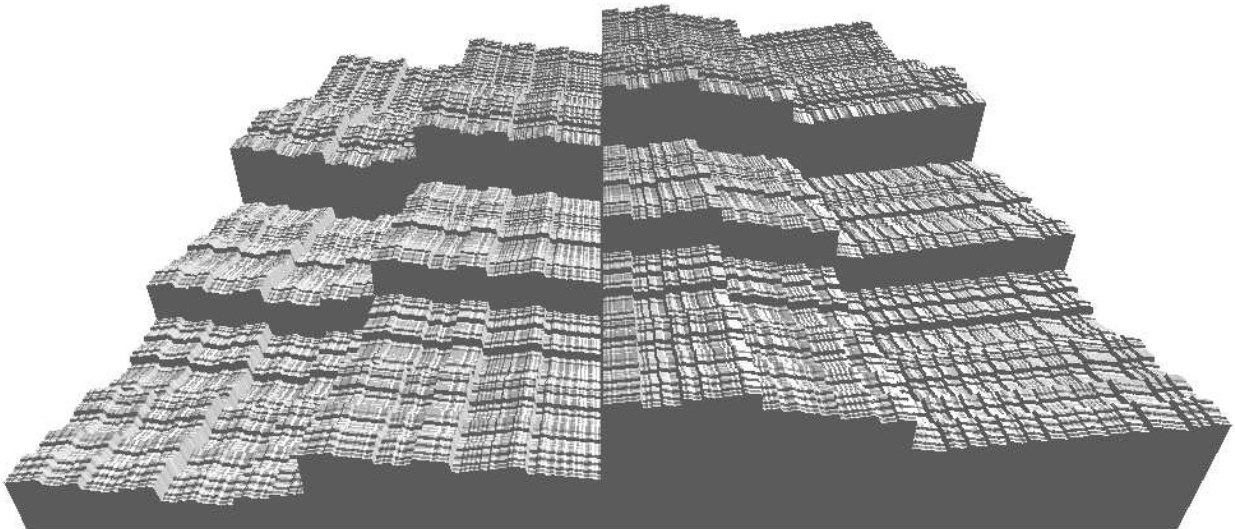


Figure 5 Randomly reversing bifurcation surface roughness

Figures 4 and 5 show squared Gray and random-roughness corresponding to Figures 1 and 3 respectively. These look like faulted and weathered granite outcroppings.

Figure 6 shows squared wiggly roughness corresponding to Figure 2. Unnatural in appearance, it resembles tire treads.

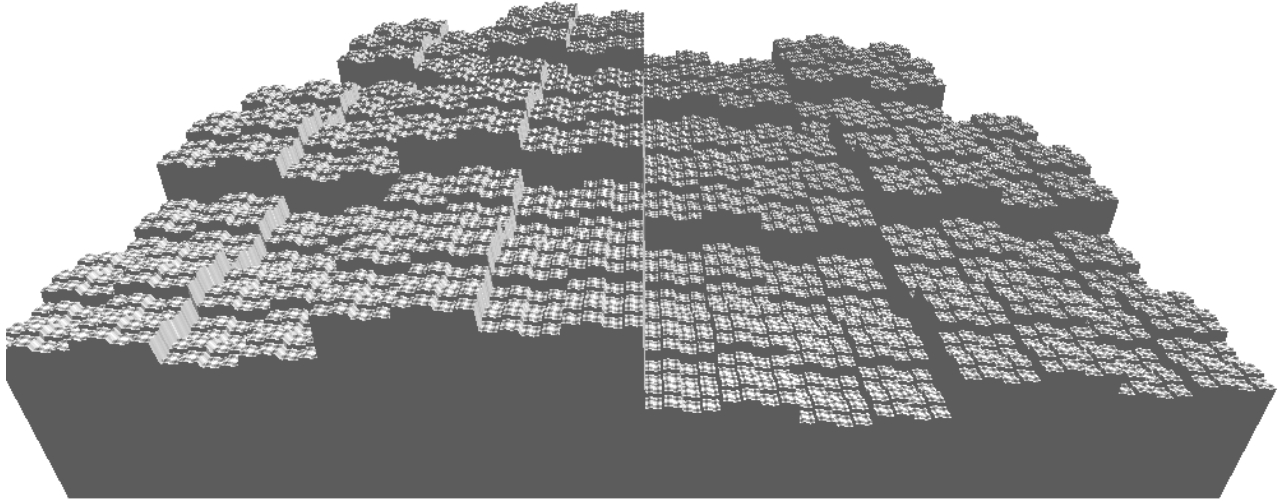


Figure 6 Wiggliest self-similar surface roughness

6. Vertical Roughness Travel

For roughness profile $Y(x, w)$, the sum of the lengths of all horizontal segments is $w - 1 = 2^j - 1$. The sum of the absolute value of the length of each vertical segment is:

$$\sum_{x=0}^{2^j-2} |Y(x, 2^j) - Y(x+1, 2^j)| \quad (8)$$

If a point were to trace a roughness profile $Y(x, w)$ from $x = 0$ to $x = w - 1$, then $w - 1$ is the horizontal distance it would travel, while formula (8) is the vertical distance.

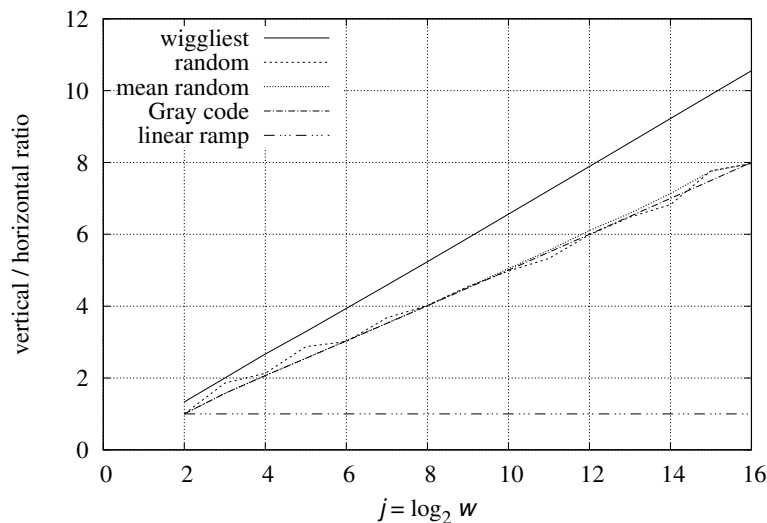


Figure 7 Vertical Travel of Roughness

Shown in Figure 7 is the of vertical to horizontal travel ratio versus j , the base-2 logarithm of w . While the slope of $1/2$ is the same for the Gray and random cases, it is $2/3$ for the wiggliest roughness W . And the vertical segments in Figure 2 are indeed longer than the vertical segments in Figures 1 and 3.

Wiggliest roughness profile $W(x, w)$ is an extreme case; it reverses vertical direction at each increment of x . For each wiggliest roughness profile there are many more random bifurcation roughness profiles. Going forward $W(x, w)$ will be ignored as an outlier.

From Figure 7 the vertical to horizontal travel ratio for the Gray and random sequences is close to:

$$\frac{j}{2} = \frac{\log_2 w}{2} \quad (9)$$

Formula (9) is unbounded as w increases. At some scale of w , vertical fluid movement by a distance of L/w will induce negligible turbulence. The argument to \log_2 must be dimensionless. $\log_2(\epsilon/L)$ is always negative because $\epsilon \ll L$; $\log_2(L/\epsilon)$ is positive, but inverts the sense of formula (9). Letting $w = L/\epsilon$, the ratio of vertical to horizontal travel is then:

$$\frac{2}{\log_2(L/\epsilon)} \quad (10)$$

The peak-to-valley height is $\sqrt{12}$ times the RMS height-of-roughness ϵ . So the vertical to horizontal ratio should be scaled:

$$\frac{1}{\sqrt{12}} \frac{2}{\log_2(L/\epsilon)} = \frac{1}{\sqrt{3} \log_2(L/\epsilon)} \quad (11)$$

The base-2 logarithm is an artifact of the discrete roughness functions from Section 4. The analogous mean field theory is to treat $Z = |\Delta Y|$ as a continuous random variable in a Pareto distribution where the frequency of Z is inversely proportional to Z^2 :

$$1 / \left[\int_{\epsilon}^L \frac{\sqrt{3} Z}{Z^2} dZ \right] = \frac{1}{\sqrt{3} \ln(L/\epsilon)} \quad (12)$$

Note that the surface height-of-roughness ϵ is used in equation (12) instead of the profile height-of-roughness ϵ in (11).

7. Skin Friction

For a rough flat surface subjected to a steady flow parallel to its surface which is sufficiently fast to generate turbulence, the skin-friction drag is the pressure opposing the flow due to viscous dissipation of that turbulence. As the height of roughness ϵ grows relative to the characteristic-length L , pressure drag (which is not dissipative) grows. $L/\epsilon \gg 1$ constrains the system so that skin-friction drag dominates pressure drag.

The skin-friction coefficient f_c is the ratio of the shear stress τ , which is the skin-friction drag in this case, to the flow kinetic energy density $\rho u^2/2$.

$$f_c = \frac{\tau}{\rho u^2/2} \quad (13)$$

f_c is dimensionless; both τ and $\rho u^2/2$ have units of pressure, $\text{kg}/(\text{m s}^2)$. Because the system as a whole can't dissipate more energy per mass than is available from the kinetic energy density, $0 < f_c < 1$.

Scaling by the vertical to horizontal travel ratio from formula (12) converts a horizontal velocity u to a vertical roughness velocity u_R , from which τ is derived:

$$u_R = \frac{u}{\sqrt{3} \ln(L/\epsilon)} \quad \tau = \frac{\rho u_R^2}{2} = \frac{\rho u^2}{6 \ln^2(L/\epsilon)} \quad (14)$$

Combining equations (14) and (13) produces a formula for f_c dependent only on L/ϵ :

$$f_c = \frac{1}{3 \ln^2(L/\epsilon)} \quad (15)$$

Figure 8 plots f_c over two decades of L/ϵ .

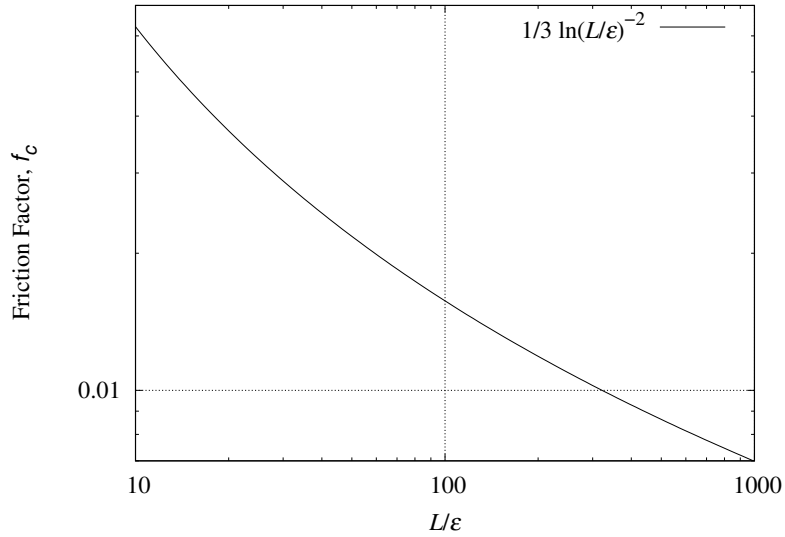


Figure 8 Skin-Friction Coefficient versus Relative Roughness

The Chilton and Colburn J-factor analogy (16) relates friction factors to turbulent forced convective heat transfer.

$$\text{Nu} = \frac{f_c}{2} \text{Re Pr}^{1/3} \quad (16)$$

Combining equation (16) with equation (15) yields a correlation for forced convection:

$$\text{Nu} = \frac{\text{Re Pr}^{1/3}}{6 \ln^2(L/\epsilon)} \quad (17)$$

8. Self-Dissimilar Roughness

Do equations (15) and (17) apply only to surfaces with self-similar roughness?

The Convection Machine[7] bi-level plate surface was composed of (676) $8.28 \text{ mm} \times 8.28 \text{ mm} \times 6 \text{ mm}$ posts spaced on 11.7 mm centers. The area of the top of each post is 0.686 cm^2 , half of the 1.37 cm^2 cell. The arithmetic-mean (also the root-mean-squared) height-of-roughness was thus 3 mm. This is the roughest surface which can be constructed in a 6 mm vertical span. And this plate surface has no self-similarity.⁵

The vertical to horizontal travel ratio of the bi-level profile would be $52 \times 0.006/0.305 = 1.023$, which, being larger than 1, would dissipate more energy per mass than is available from the kinetic energy density. Applying formula (15) instead produces a f_c value of 0.0216. The corresponding convection correlation (17) trace “Rough Turbulent Asymptote 3.0 mm” in Figure 9 matches the “3.0 mm $\Delta T=11\text{K}$ Measured” convection within $\pm 3\%$ from $\text{Re} = 5000$ to 50000.

This is strong evidence that formulas (15) and (17) are intrinsic to roughness and not specific to self-similar profiles. The factor of $1/3$ in formula (15) derives from $\sqrt{12}$ in equation (5). That is strong evidence that root-mean-squared height-of-roughness is the correct metric for roughness.

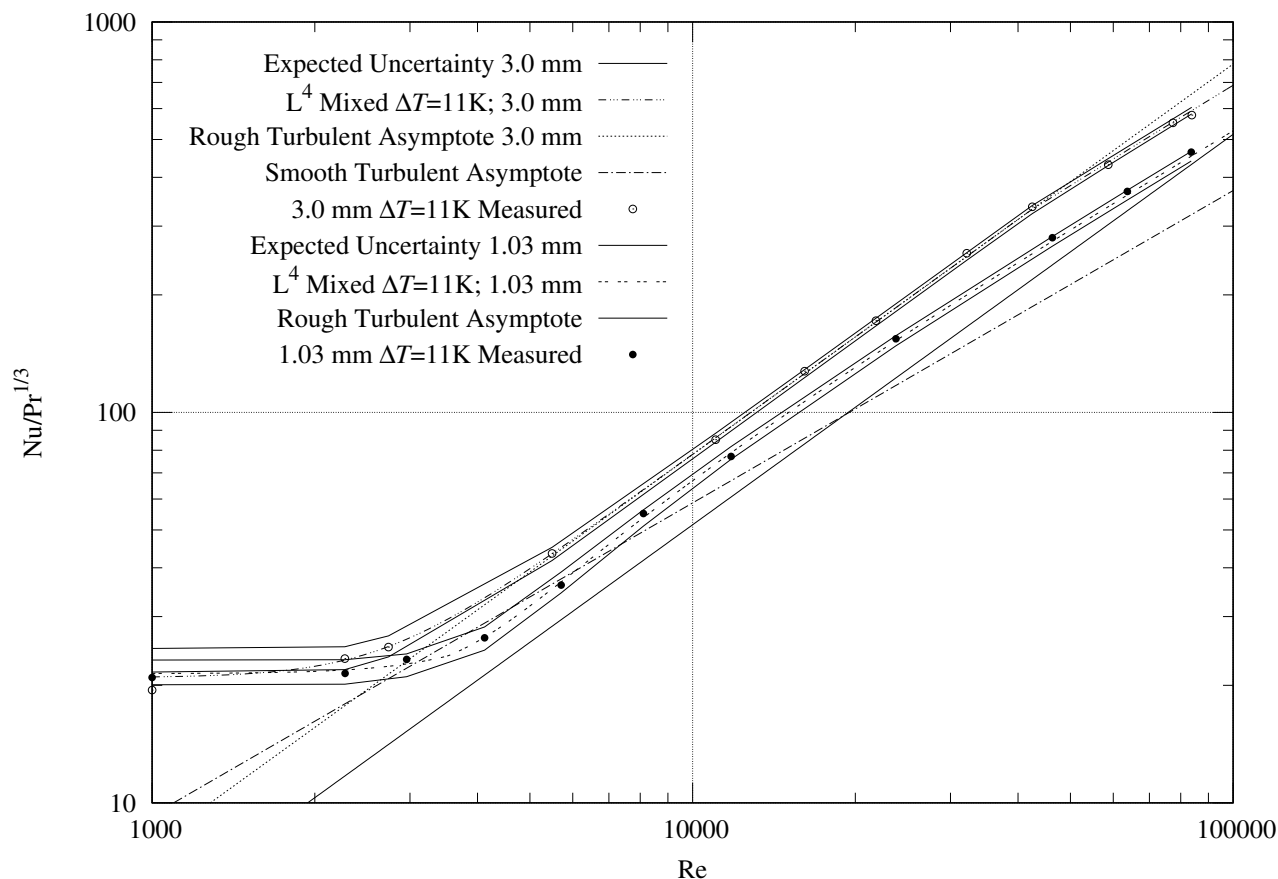


Figure 9 Convection and Measurement Uncertainties from Rough Plates

Figure 9 compares the measurements for the downward-facing plates with equations (17) and (26) and their predicted uncertainties calculated for each measurement. At $\text{Re} < 5000$ the curves for equation (26) are corrected for mixed convection, as described in *Turbulent Mixed Convection from an Isothermal Plate*[8].

The traces not labeled “asymptote” in Figures 9 and 10 are using a more sophisticated model developed in Section 17 for the bi-level plate transition between rough turbulent and smooth turbulent convection taking place on the post tops. Figure 10 shows that the percentage discrepancy from the “rough-smooth transition” model is within $\pm 2\%$ for $6000 < \text{Re} < 80000$.

⁵ Self-similarity is similarity between shape at different scales; but these blocks are all the same size.

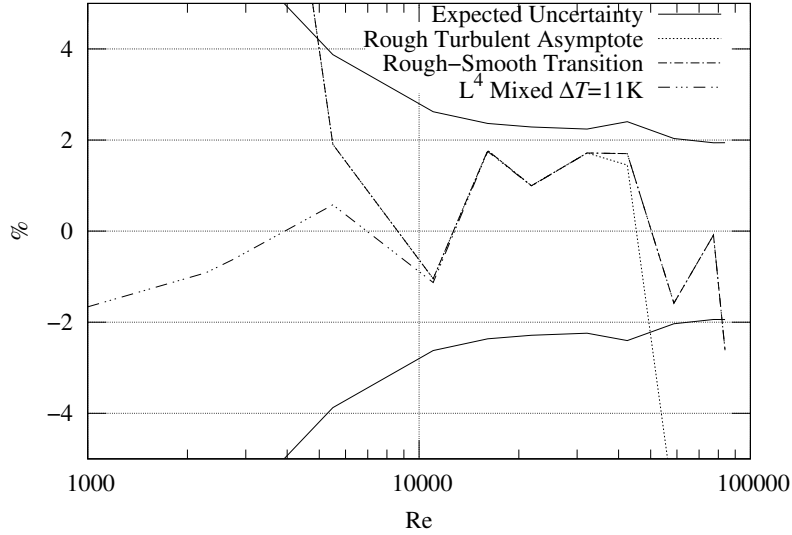


Figure 10 Measurement versus Theory of 3.0 mm Roughness Plate

9. Transitional Rough Regime

Afzal, Seena, and Bushra[9] (and Schlichting[2]) relate that the internal roughness of commercial pipes behaves differently from Nikuradse’s sand coated pipes. While the curves for commercial pipes are monotonically decreasing on the Moody diagram, the diagram for Nikuradse’s pipes are not monotonic, which they term inflectional.⁶ The total coefficient of resistance (c_f) Moody diagram from Prandtl and Schlichting[1] shows a 10% dip spread over one and a half decades of Re just to the right of the smooth skin-friction line for each horizontal trace.

For a self-similar roughness, there should be no variation in skin-friction for Reynolds numbers larger than that associated with the plate’s admissible-roughness (discussed in Section 11):

$$Re > \frac{29 L}{\varepsilon_{pv}} \approx 1474$$

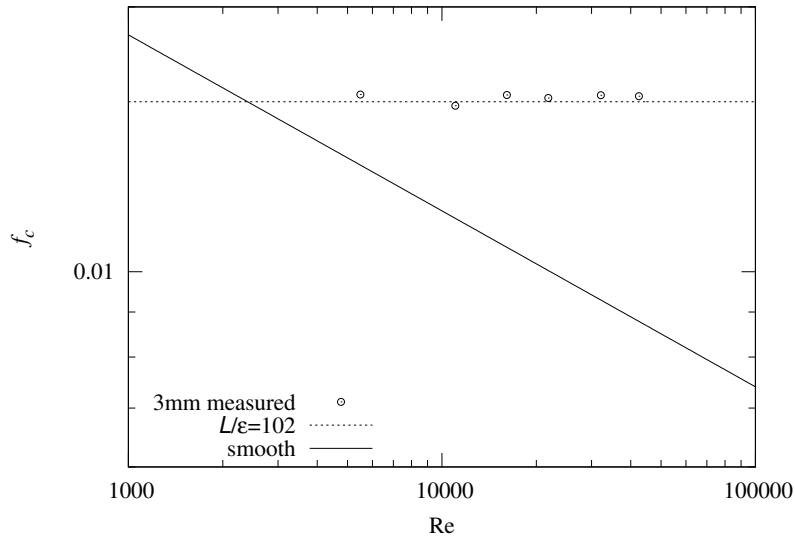


Figure 11 f_c vs. Re for 3 mm Roughness Plate

⁶ Afzal, Seena, and Bushra introduce a second parameter to model both behaviors.

Figure 11 is a Moody diagram of the 3 mm roughness bi-level plate measurements converted to friction coefficients f_c using the Chilton and Colburn J-factor analogy (16). The “3 mm measured” points hew closely to the “ $L/\varepsilon = 102$ ” line and are flat within the expected measurement uncertainties.

With the skin-friction of self-similar roughness independent of Re , and the roughest (self-dissimilar) surface which can be constructed (bi-level plate) also having no dependence on Re , the skin-friction formula (15) applies over the full range of turbulent flow. This is much simpler than rough pipe interiors, which depend on Re except in “the completely rough regime”. This is discussed further in Section 12.

10. Sand Roughness

Modeling sand grains as unit radius spheres glued to the plate surface in a square array and modeling the space not covered by a sphere as glue of height $0 \leq \bar{g} \leq 1$, the mean height of the enclosing square cell of area A containing a unit sphere is:

$$\bar{z} = \left(\int_0^1 2\pi x \left(\sqrt{1-x^2} + 1 \right) dx + (A - \pi)\bar{g} \right) / A = \left(\frac{5}{3}\pi + (A - \pi)\bar{g} \right) / A$$

The (dimensionless for unit radius sphere) arithmetic-mean height-of-roughness R_a and the root-mean-squared height-of-roughness R_q are:

$$2 R_a = \left(\int_0^1 2\pi x \left| \sqrt{1-x^2} + 1 - \bar{z} \right| dx + (A - \pi) |\bar{z} - \bar{g}| \right) / A$$

$$2 R_q = \sqrt{ \left(\int_0^1 2\pi x \left(\sqrt{1-x^2} + 1 - \bar{z} \right)^2 dx + (A - \pi) (\bar{z} - \bar{g})^2 \right) } / A$$

For glue level $1 < \bar{g} < 2$, the grains are more than 50% submerged. Let $r_g = \sqrt{(1 - (\bar{g} - 1)^2)} = \sqrt{2\bar{g} - \bar{g}^2}$ be the radius of the glue opening through which the sphere is exposed. The mean height of the enclosing square cell of area A containing a unit sphere is then:

$$\bar{z} = \left(\int_0^{r_g} 2\pi x \left(\sqrt{1-x^2} + 1 \right) dx + (A - \pi r_g^2) \bar{g} \right) / A = \left(\frac{4 + 3\bar{g}^2 - 2\bar{g}^3}{3} \pi + (A - \pi r_g^2) \bar{g} \right) / A$$

For this submerged case, R_a and R_q are:

$$2 R_a = \left(\int_0^{r_g} 2\pi x \left| \sqrt{1-x^2} + 1 - \bar{z} \right| dx + (A - \pi r_g^2) |\bar{z} - \bar{g}| \right) / A$$

$$2 R_q = \sqrt{ \left(\int_0^{r_g} 2\pi x \left(\sqrt{1-x^2} + 1 - \bar{z} \right)^2 dx + (A - \pi r_g^2) (\bar{z} - \bar{g})^2 \right) } / A$$

Figure 12 shows the conversion factor from ε to k_S as a function of relative glue thickness.

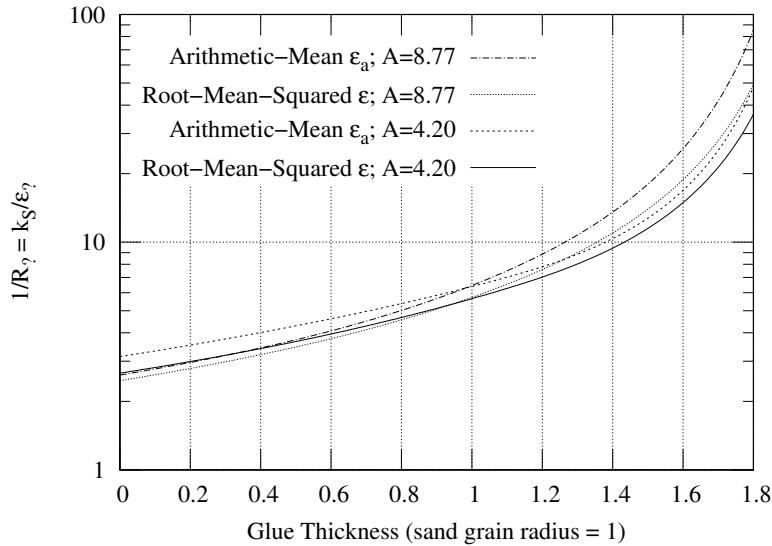


Figure 12 ε_a and ε to k_S conversion factors vs. Glue Thickness and Cell Area A

In order to compare the Prandtl and Schlichting[1] formula (1) with formula (15) of present work, different k_S/ε conversion factors (and relative glue thicknesses) must be used at large and small k_S values.

The unit cell area for the larger grains is 4.2. With $L/\varepsilon = 150$, compare $4c_f$ for $L/k_S = L R_a/\varepsilon$ in Table 2 and $L/k_S = L R_q/\varepsilon$ in Table 3 with $f_D = 0.0528$ calculated from equation (15):

Table 2 Average roughness R_a versus large-grain sand-roughness k_S				
\bar{g}	\bar{z}	$1/R_a$	L/k_S	$4c_f$
0.00	1.25	3.14	47.7	0.088
0.70	1.42	4.97	30.2	0.105
1.00	1.50	6.38	23.5	0.117

Table 3 RMS roughness R_q versus large-grain sand-roughness k_S				
\bar{g}	\bar{z}	$1/R_q$	L/k_S	$4c_f$
0.00	1.25	2.66	56.4	0.082
0.87	1.47	4.98	30.1	0.105
1.00	1.50	5.64	26.6	0.111

$f_D = 0.0528$ is out of the range of possible $4c_f$ values for arithmetic-mean and RMS roughness with $\bar{g} \geq 0$. However, there are values of $4c_f/2$ which are within range for both RMS and arithmetic-mean roughness.

A factor of 2 is introduced in the last step of Prandtl and Schlichting's paper[1]. While it is justified for the local coefficient of resistance, the reason for its presence in the total coefficient of resistance is difficult to discern through so many changes of variables.

In their example of the use of their formula, Mills and Hang[4] divide C_D by 2.

Half the $4c_f$ value from the $\bar{g} = 0.70$ row in Table 2 matches $f_D = 0.0528$, as does the $\bar{g} = 0.87$ row in Table 3, for arithmetic-mean and RMS height-of-roughness respectively.

The unit cell area for the smaller grains is 8.77. The largest pipe which Nikuradse tested had a diameter of 0.101 m. With a coating made from the smallest sand grain size (.01 cm), $L/k_S = 1014$ and the corresponding $f_D = 0.0277$. As before, there is no glue level $\bar{g} \geq 0$ whose $4c_f$ matches f_D , but half of $4c_f$ does match at $\bar{g} = 0.90$ and $\bar{g} = 0.99$ in Tables 4 and 5.

Table 4 Average roughness R_a versus small-grain sand-roughness k_S				
\bar{g}	\bar{z}	$1/R_a$	L/k_S	$4c_f$
0.00	0.60	2.61	388.6	0.044
0.90	1.17	5.65	179.4	0.055
1.50	1.57	17.98	56.4	0.082

Table 5 RMS roughness R_q versus small-grain sand-roughness k_S				
\bar{g}	\bar{z}	$1/R_q$	L/k_S	$4c_f$
0.00	0.60	2.46	411.4	0.043
0.99	1.23	5.65	179.4	0.055
1.50	1.57	13.95	72.7	0.075

Afzal, Seena, and Bushra in *Turbulent flow in a machine honed rough pipe for large Reynolds numbers: General roughness scaling laws*[9] fit 5.333 for the RMS to sand-roughness conversion factor and 6.45 for the arithmetic-mean to sand-roughness conversion factor. The mean of the $1/R_q$ values 4.98 and 5.65 is within 1% of 5.333 (and not close to 6.45). This is strong evidence that RMS height-of-roughness is the true metric for surface roughness.

In *Skin-friction behavior in the transitionally-rough regime*[6], Flack, Schultz, Barros, and Kim measure skin-friction from grit-blasted surfaces. They find "The root-mean-square roughness height (k_{rms}) is shown to be most strongly correlated with the equivalent sand roughness height (k_S) for the grit-blasted surfaces."

Figure 13 shows that the corrected Mills-Hang formula (2) is nearly coincident with the equation (15) over the range $100 < L/\varepsilon < 1000$; so it is an improvement over Prandtl and Schlichting's correlation (1). At $L/\varepsilon > 1000$, the inset in Figure 13 shows that both suffer from the scale error discussed in Section 2, growing to -13% and -18% relative to the equation (15) trace at $L/\varepsilon = 10^6$.

The 3 mm RMS roughness plate has an equivalent sand-roughness of 16 mm; $L/\varepsilon = 102$; $L/k_S = 19.1$

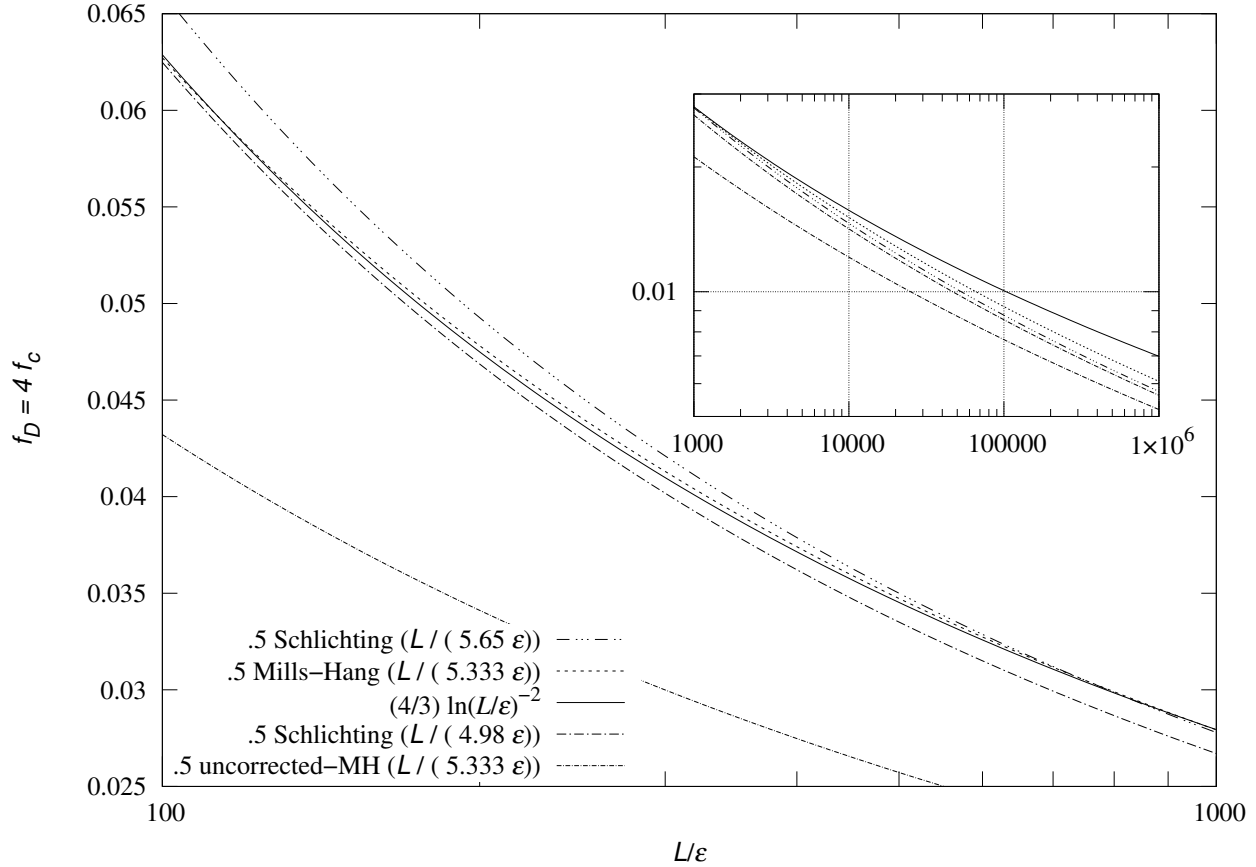


Figure 13 Fully Rough (Turbulent) Darcy Friction Factor

11. Admissible Roughness

“The amount of roughness which is considered “admissible” in engineering applications is that maximum height of individual roughness elements which causes no increase in drag compared with a smooth wall.”⁷ Schlichting[2] develops a formula for k_{adm} from its Fig. 21.9. (Resistance formula of sand-roughened plate; coefficient of *total* skin friction):

$$u k_{adm} / \nu = 100 \quad (18)$$

A footnote states “The estimates performed in this section make no distinction between the equivalent sand height, k_S , and the actual height, k , of a protuberance.” In the Section 10 model of sand-roughness, the protuberance height is $(1 - \bar{g}/2) k_S$. For Nikuradse’s large grains that is $0.57 k_S$; for small grains it is $0.51 k_S$. So equation (18) overestimates the admissible-roughness height.

For a given RMS roughness ϵ , the equal-area bi-level plate has the smallest possible protuberance height $k = 2\epsilon$; while large-grain sand-roughness would have $k = 0.57 \times 5.333\epsilon = 3.0\epsilon$ and small-grain $k = 0.51 \times 5.333\epsilon = 2.7\epsilon$.

The goal is to find the Re value in the 1.03 mm trace in Figure 9 below which the slope of measured $\text{Nu}/\text{Pr}^{1/3}$ is 4/5. Natural convection obscures the slope below $\text{Re} = 4419$; at best an upper bound can be found. This upper bound for k_{adm} in equation (19) is a significant reduction from equation (18):

$$k \frac{\text{Re}}{L} = 0.002 \frac{4419}{0.305} \approx 29.0 \quad k_{adm} = 29 \frac{\nu}{u} = 29 \frac{L}{\text{Re}} \quad (19)$$

⁷ This definition does not imply that roughness always causes an increase in drag; for example in Figure 9 the 1 mm roughness curve is less than the smooth-turbulent asymptote from $3000 < \text{Re} < 7000$.

12. Roughness in Pipes

Applying self-similar roughness to pipe interiors is difficult because, while the isobaric plate environment allows roughness to grow proportionally to L , the boundary-layer runs out of room inside cylindrical pipes. Looking at roughness more generally may provide some insights.

The skin-friction of plate roughness being independent of Re is evidence that the monotonic/inflective variation in pipe skin-friction with Re is not due to some property of isotropic surface roughness. Commercial pipe interiors might well have longitudinal roughness different from circumferential roughness as a result of their manufacturing processes, for instance extrusion.

Assuming Nikuradse's sand-roughness samples had isotropic roughness, why aren't their Moody diagram traces flat? The characteristic-length for pipe-flow is the diameter of the pipe; but the bulk flow is longitudinal. It is not clear that the longitudinal roughness should be measured against the same characteristic-length as the circumferential roughness. If the characteristic-lengths should be different, then pipe skin-friction should be formulated as a function of the circumferential and longitudinal profile roughnesses (and Re) instead of a single surface roughness (and Re).

13. Conclusion

- For flat plates with roughness well distributed over the surface with RMS height-of-roughness $\varepsilon \ll L$ (and the peak-to-valley distance $\varepsilon_{pv} > 29 L/Re$):

$$f_c = \frac{1}{3 \ln^2(L/\varepsilon)} \quad Nu = \frac{Re Pr^{1/3}}{6 \ln^2(L/\varepsilon)}$$

- Convection measurements of a bi-level isothermal plate having precisely 3 mm of roughness match the convection correlation within 3% at Reynolds numbers from 5000 to 50000.
- $k_{adm} = 29 L/Re$ is an upper bound for admissible-roughness, the maximum protuberance height which causes no increase in drag compared with a smooth plate.
- To convert between RMS height-of-roughness ε and sand-roughness k_S : $k_S \approx 4.98 \varepsilon$ for Nikuradse's large sand-grain samples and $k_S \approx 5.65 \varepsilon$ for his small sand-grain samples. If in doubt, use $k_S \approx 5.333 \varepsilon$.

14. Nomenclature

Nu	= Nusselt number
Pr	= Prandtl number
Re	= Reynolds number
Re_M	= mode threshold Reynolds number
Re_t	= transition threshold Reynolds number
Re_x	= local Reynolds number
A	= area of square cell containing sphere sand grain (m^2)
C_D	= Mills and Hang friction coefficient
c_f	= Prandtl and Schlichting friction coefficient
f_c	= friction coefficient
\bar{g}	= height of glue
$G(x, w)$	= Gray-code profile function
$j = \log_2 w$	= positive integer
k	= protuberance height (m)
k_{adm}	= height of admissible roughness (m)
k_S	= sand-roughness (m)
L	= plate characteristic-length (m)
L_S	= post characteristic-length (m)
n	= branching factor of profile roughness function
R_a	= dimensionless arithmetic-mean height-of-roughness
R_q	= dimensionless RMS height-of-roughness
r_g	= radius of glue opening exposing sphere sand grain (m)
S_S	= post center spacing on bi-level plate (m)
u	= fluid velocity (m/s)
u_R	= vertical roughness fluid velocity (m/s)
u_y	= fluid velocity at elevation y (m/s)
$w = 2^j$	= integer power of two
$W(x, w)$	= wiggliest integer self-similar profile function
$Y(x, w)$	= integer self-similar profile function
x, y	= distance (m)
$z(x)$	= profile roughness function (m)
$z(x, y)$	= surface roughness function (m)
\bar{z}	= mean height of roughness
Z	= profile roughness function random variable

15. Greek Symbols

δ	= turbulent boundary-layer depth (m)
δ_t	= thermal boundary-layer depth (m)
ϵ	= RMS profile height-of-roughness (m)
ε	= RMS surface height-of-roughness (m)
ε_a	= arithmetic-mean height-of-roughness (m)
ε_{pv}	= peak-to-valley height-of-roughness (m)
ν	= fluid kinematic viscosity (m^2/s)
ρ	= fluid density (kg/m^3)
τ	= fluid shear stress (N/m^2)
χ	= local convection for post side slice

16. References

- [1] L. Prandtl and H. Schlichting. *The Resistance Law for Rough Plates*. Translation (David W. Taylor Model Basin). Navy Department, the David W. Taylor Model Basin, 1934. Translated 1955 by P.S. Granville.
- [2] Hermann Schlichting, Klaus Gersten, Egon Collaborateur. Krause, Herbert Collaborateur. Oertel, and Katherine Mayes. *Boundary-layer theory*. Springer, Berlin, Heidelberg, Paris, 2000. Corrected printing 2003.
- [3] Mitchell G. Newberry and Van M. Savage. Self-similar processes follow a power law in discrete logarithmic space. *Phys. Rev. Lett.*, 122:158303, Apr 2019.
- [4] A. F. Mills and Xu Hang. On the skin friction coefficient for a fully rough flat plate. *J. Fluids Eng*, 105(3):364–365, 1983.
- [5] M. M. Pimenta, R. J. Moffat, and W. M. Kays. *The Turbulent Boundary Layer: An Experimental Study of the Transport of Momentum and Heat with the Effect of Roughness*. Department of Mechanical Engineering, Stanford University, 1975.
- [6] Karen A Flack, Michael P Schultz, Julio M Barros, and Yechan C Kim. Skin-friction behavior in the transitionally-rough regime. *International Journal of Heat and Fluid Flow*, 61:21–30, 2016.
- [7] A. Jaffer. Convection measurement apparatus and methodology, 2019. [Online; accessed 13-January-2019].
- [8] A. Jaffer. Turbulent mixed convection from an isothermal plate, 2019. [Online; accessed 13-January-2019].
- [9] Noor Afzal, Abu Seena, and A. Bushra. Turbulent flow in a machine honed rough pipe for large reynolds numbers: General roughness scaling laws. *Journal of Hydro-environment Research*, 7(1):81–90, 2013.
- [10] J.H. Lienhard IV and J.H. Lienhard V. *A Heat Transfer Textbook*. Phlogiston Press, Cambridge, MA, 4th edition, 2018. Version 2.12.

17. Appendix: Rough to Smooth Turbulence Transition

The roughness of the bi-level plate is not self-similar; it exhibits different convection behaviors at different scales. The slope of the upper end of both curves in Figure 9 is 4/5, but with a magnitude possible only if operating with a much shorter characteristic-length than the plate's $L = 0.305$ m.

At the leading edge of the plate, the smooth-turbulent boundary-layer depth would be much smaller than the height-of-roughness; so fully rough convection (17) applies. The turbulent boundary-layer depth increases with distance x from the leading edge:

$$\delta(x) = \frac{0.37 x}{\text{Re}_x^{1/5}} = 0.37 x^{4/5} \left(\frac{L}{\text{Re}} \right)^{1/5} = 0.37 L \frac{\text{Re}_x^{4/5}}{\text{Re}} \quad (20)$$

Solving for Re_x where $\delta = \varepsilon_{pv}$, the peak-to-valley height:

$$\text{Re}_x = \left(\frac{\varepsilon_{pv}}{L} \frac{\text{Re}}{0.37} \right)^{5/4}$$

In the Convection Machine[7] data it seems that around

$$\text{Re}_x > \frac{\varepsilon_{pv}}{L_S} \left(\frac{\varepsilon_{pv}}{L} \frac{121 \times 10^3}{0.37} \right)^{5/4} \quad (21)$$

the flow transitions to a regime consisting of smooth turbulent convection (22) from the channels between posts at scale L and smooth turbulent convection (22) from the post at scale $L_S = 8.3$ mm, the length of the post in the direction of flow.

$$\text{Nu} = 0.037 \text{Re}^{4/5} \text{Pr}^{1/3} \quad (22)$$

Where $S_S = L/26$ is the post center spacing, the longitudinal (parallel to flow) channels between the posts have convection:

$$\text{Nu}_C / \text{Pr}^{1/3} = \frac{S_S - L_S}{S_S} 0.037 \text{Re}^{4/5} \quad (23)$$

The top of the posts occupy half (L_S^2/S_S^2) of the plate area; their convection is:

$$\text{Nu}_T / \text{Pr}^{1/3} = \frac{L_S^2}{S_S^2} \left(\frac{L}{L_S} \right)^{1/5} 0.037 \text{Re}^{4/5} \quad (24)$$

The $(L/L_S)^{1/5}$ factor converts the characteristic-length from L_S to L .

Both post sides parallel to the flow also experience smooth turbulent convection at scale $L_S = 8.3$ mm, but because the sides are within the channel's boundary layer, temperature and velocity are not constant with elevation. The channel velocity profile provides velocity as a function of elevation y , boundary layer depth δ , and free stream velocity u :

$$\frac{u_y}{u} = \begin{cases} (y/\delta)^{1/7} & \text{when } y \leq \delta; \\ 1, & \text{otherwise.} \end{cases}$$

By analogy with the derivation of the thermal profile for laminar flow from Lienhard and Lienhard[10], the turbulent thermal profile would be:

$$\frac{T - T_w}{T_\infty - T_w} = \begin{cases} (y/\delta_t)^{1/7} & \text{when } y \leq \delta_t; \\ 1, & \text{otherwise.} \end{cases} \approx \begin{cases} \left(y / \left(\delta \text{Pr}^{-1/3} \right) \right)^{1/7} & \text{when } y \leq \delta; \\ 1, & \text{otherwise.} \end{cases}$$

The temperature profile will affect side convection by a factor of approximately $\text{Pr}^{1/21} (y/\delta)^{1/7}$ when $y \leq \delta$; and 1 otherwise. In air, $\text{Pr}^{1/21}$ is a reduction by 1.5% (for the post sides convection only).

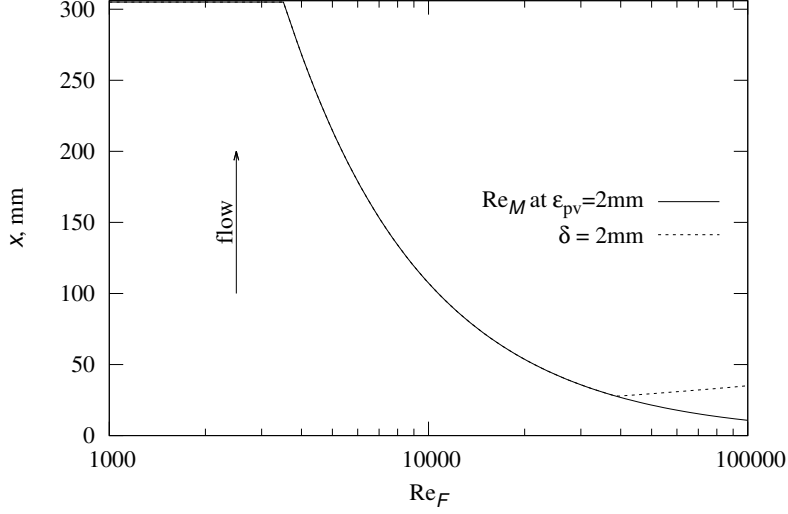


Figure 14 Convection Mode Regions versus Reynolds number

Each vertical slice of Figure 14 represents the regions of convection on the surface of the 1 mm roughness plate at the indicated value of Re . The entire surface is in rough turbulent convection of correlation (17) below the Re_M trace where (21) is not satisfied. Above the Re_M trace, the convection is modeled as a combination of channel (23), post-top (24), and post-side (25) convection. When Re is larger than 40000, there is a small region where the channel boundary-layer height is smaller than the post side height $\varepsilon_{pv} = 2$ mm. Post side convection from this region was modeled, but its effect on total convection was negligible. For simplicity, the post side model uses formula (25) for all post side convection.

The convection for a vertical slice of the post side is:

$$\begin{aligned}
 \chi(x) &= \frac{0.037}{\varepsilon_{pv}} \int_0^{\varepsilon_{pv}} \left(\frac{y}{\delta(x) \text{Pr}^{-1/3}} \right)^{1/7} \left(\text{Re}_x \left(\frac{y}{\delta(x)} \right)^{1/7} \right)^{4/5} dy \\
 &= \frac{0.037 \text{Pr}^{1/21}}{\varepsilon_{pv}} \int_0^{\varepsilon_{pv}} \left(\frac{y}{0.37 x^{4/5} \left(\frac{Re}{L} \right)^{1/5}} \right)^{1/7} \left(\frac{Re x}{L} \left(\frac{y}{0.37 x^{4/5} \left(\frac{Re}{L} \right)^{1/5}} \right)^{1/7} \right)^{4/5} dy \\
 &= 0.038 \frac{\text{Re}^{149/175} \text{Pr}^{1/21} x^{113/175} \varepsilon_{pv}^{9/35}}{L^{158/175}}
 \end{aligned}$$

The convection from a row of post sides in line with the flow is:

$$\begin{aligned}
 \text{Nu}/\text{Pr}^{1/3} &= 2 \frac{\varepsilon_{pv} L_S}{S_S^2} \left(\frac{L}{L_S} \right)^{1/5} \frac{1}{L} \int_0^L \chi(\varepsilon_{pv}) dx \\
 &= 2 \frac{\varepsilon_{pv} L_S}{S_S^2} \left(\frac{L}{L_S} \right)^{1/5} 0.0231 \text{Pr}^{1/21} \left(\frac{\varepsilon_{pv}}{L} \right)^{9/35} \text{Re}^{149/175}
 \end{aligned} \tag{25}$$

Integrating the local convections for correlations (17), (23), (24), and (25) over distance:

$$\begin{aligned}
 \text{Re}_M &= \min \left(\text{Re}, \frac{\varepsilon_{pv}}{L_S} \left(\frac{\varepsilon_{pv}}{L} \frac{\text{Re}_t}{0.37} \right)^{5/4} \right) \quad \text{Re}_t = 121 \times 10^3 \\
 \text{Nu}/\text{Pr}^{1/3} &= \frac{\text{Re}_M}{6 \ln^2(\varepsilon/L)} + \left[\frac{S_S - L_S}{S_S} + \frac{L_S^2}{S_S^2} \left(\frac{L}{L_S} \right)^{1/5} \right] 0.037 \left(\text{Re}^{4/5} - \text{Re}_M^{4/5} \right) \\
 &\quad + 2 \frac{\varepsilon_{pv} L_S}{S_S^2} \left(\frac{L}{L_S} \right)^{1/5} 0.0231 \text{Pr}^{1/21} \left(\frac{\varepsilon_{pv}}{L} \right)^{9/35} \left(\text{Re}^{149/175} - \text{Re}_M^{149/175} \right)
 \end{aligned} \tag{26}$$

The constant Re_t adds a degree of freedom to the plate model; but Figure 9 shows that $Re_t = 121000$ fits both 3 mm roughness and 1 mm roughness data-sets within their estimated uncertainties below $Re = 80000$. Figure 10 shows that the percentage discrepancy from the mixed model for 3 mm roughness is within $\pm 2\%$ below $Re = 80000$.

While the L^4 Mixed and Rough Turbulent Asymptote traces for 3 mm roughness are close in Figure 9, those traces for 1 mm roughness are not. This is because when ε of the plate was reduced from 3 mm to 1 mm, L_S was not similarly scaled.